SPACE RESEARCH COORDINATION CENTER

NIGHTGLOW SPECTRAL LINE SHAPES OF OXYGEN λ6300 AND λ5577 RADIATION

BY

MANFRED A. BIONDI AND WALTER A. FEIBELMAN

DEPARTMENT OF PHYSICS

SRCC REPORT NO. 56

UNIVERSITY OF PITTSBURGH

PITTSBURGH, PENNSYLVANIA

2 OCTOBER 1967

Nightglow Spectral Line Shapes of Oxygen λ6300 and λ5577 Radiation

Manfred A. Biondi and Walter A. Feibelman

(Planetary and Space Sciences)

University of Pittsburgh

Pittsburgh, Pennsylvania

September 1967

Nightglow Spectral Line Shapes of Oxygen λ6300 and λ5577 Radiation*

Manfred A. Biondi and Walter A. Feibelman

Physics Department

University of Pittsburgh

Pittsburgh, Pa.

Abstract

A pressure-tuned Fabry-Perot interferometer employing photoelectric detection has been used to measure the oxygen λ6300 and λ5577 spectral line profiles during twilight and the night at the Airglow Observatory on Laurel Mountain, Pennsylvania. The inferred O(^{1}D) atom temperatures, ranging from ~600 - 1600°K, are compared with the predicted temperature variations using empirical models relating solar activity to exospheric heating, and agreement is found on some nights, while substantial discrepancies (~400°K) are found on others. No evidence for a dissociative origin of the ^{1}D or ^{1}S oxygen atoms has been detected in the line profiles obtained to date; however, there is a possible indication of F-layer wind velocities of ~400 m/s.

---

*This research was supported, in part, by the National Science Foundation, Atmospheric Sciences Division (Aeronomy), GP-4435, and the Office of Naval Research, Nonr-624(13).

I. Introduction

The present experimental investigation was undertaken in an attempt to clarify the nature of the excitation mechanisms for production of $O(^1D)$ atoms in the ionosphere[1, 2] by studying the spectral line profiles of the emitted λ6300 radiation. In particular, one proposed source of the night-glow λ6300 red line is dissociative recombination occurring in the F-layer with a coefficient $\alpha \sim 2 \times 10^{-7}$ cm^3/sec[3] according to the reaction,

$$O_2^+ + e \rightarrow (O_2^*)_{\text{unstable}} \begin{cases} \rightarrow O^*(^1D) + O(^3P) + E_d \\ \rightarrow O^*(^1D) + O^*(^1D) + E'_d \\ \rightarrow O^*(^1D) + O^*(^1S) + E''_d \end{cases} , \qquad (1)$$

where, as a result of the potential energy released in the reaction, the two oxygen atoms share the kinetic energy of dissociation, E_d. If the O_2^+ ions are in their ground electronic and vibrational states, then $E_d = 5.0$ eV, $E'_d = 3.1$ eV, and $E_d'' = 0.8$ eV. (If the corresponding reaction using NO^+ ions in place of O_2^+ occurs, then $E_d'' = 0.8$ eV, providing the $O^*(^1D)$ atoms with very little kinetic energy, when the NO^+ ion is in its ground state.) One may therefore hope to verify the dissociative nature of the $O^*(^1D)$ production by detecting the kinetic energy imparted to the ^1D atom by the reaction. Our conclusion that this is a reasonable possibility is based on estimates of the rates of the relevant atomic collision processes governing quenching and slowing of the excited atoms, as well as excitation transfer to the ambient ^3P ground state oxygen atoms. We also have been encouraged by the results of laboratory afterglow studies, in which dissociation kinetic energy was successfully detected[4, 5] in the radiation from excited neon and argon atoms produced by dissociative recombination of electrons with Ne_2^+ and Ar_2^+ ions.

In the present experiment the kinetic energy of the excited ^1D and ^1S oxygen atoms at the instant they radiate is studied by measuring the spectral line shapes of the emitted radiations with a photoelectric-recording, scanning Fabry-Perot interferometer of high sensitivity[6, 7]. In this respect, the measurements are somewhat similar to those reported by Jarrett and Hoey[8], although our techniques and conclusions differ from theirs in a number of points.

In the next sections we discuss the relevant atomic collision processes governing the production and destruction of the excited O atoms and consider the possible spectral line shapes which result when the atoms radiate. We then describe the experimental techniques used in the nightglow line shape determinations. Finally, we present the results of the measurements and compare them with predictions of ionospheric models relating such quantities as solar activity to ionospheric temperature.

II. Atomic Collision Processes Affecting λ6300 and λ5577 Emission

We are concerned not so much with those processes which determine the intensity of the oxygen nightglow radiations as with those which yield the velocity distributions of the excited atoms at the instant they radiate. As noted in the introduction, a principal source of nightglow λ6300 radiation is thought to be dissociative recombination, reaction (1), of O_2^+ ions and electrons[1]. Although recombination of NO^+ ions with electrons energetically can lead to ^1D oxygen atom production, difficulty with spin conservation in going from the $X^1\Sigma^+$ state of NO^+ to the ^1D oxygen and ^4S nitrogen atom states may exclude such ^1D production[9]; there is, however, no direct evidence against this process.

A second source of ^1D oxygen atoms which probably contributes during twilight is dissociative photoexcitation of neutral oxygen molecules which

leads to the Schumann-Runge absorption continuum below 1740Å and leaves one of the oxygen atoms in the ^1D excited state, i.e.

$$O_2 + h\nu \rightarrow O(^1D) + O(^3P) + E_d \quad . \tag{2}$$

A similar reaction may lead to production of $O(^1S)$ atoms[10, 11].

A third potential source of ^1D oxygen atoms during a portion of the night is impact excitation of ^3P oxygen atoms by a "hot" electron gas produced by energetic photoelectrons from the conjugate point, when that point remains in sunlight well after local sunset[12]. Thus, the reaction,

$$e_f + O(^3P) \rightarrow e_s + O(^1D) \quad , \tag{3}$$

where the subscripts f and s refer to fast and slow electrons, respectively, will produce $O(^1D)$ atoms moving with essentially the ambient neutral atom temperature.

Reaction (1) may also lead to $O(^1S)$ production. (Here recombination of electrons with NO^+ ions in their ground vibrational state does not have sufficient energy to populate the $O(^1S)$ state.) However, the λ5577 nightglow radiation, which emanates chiefly from E-layer altitudes, also may result from production of ^1S atoms in 3-body neutral atom recombination reactions involving O atoms. Here, analagous reactions for production of $O(^1D)$ atoms may occur. Since the three-body reactions are significant only in the higher density, lower altitude regions, quenching of the long-lived states may occur before radiation, and in fact, probably accounts for the lack of red-line radiation from the E-region.

Quenching may lead to destruction of the metastable $^1S(\tau_{rad} = 0.74$ sec) and $^1D(\tau_{rad} = 110$ sec) oxygen states by reactions such as,

$$O^*(^1D) + N_2 \rightarrow O(^3P) + N_2^* \quad , \tag{4}$$

where the excitation of the nitrogen molecule is probably in vibrational modes. Apparently reaction (4) exhibits a coefficient, $\beta_{quench} \sim 2 \times 10^{-11}$ cm^3/s[13], in which case quenching would compete with radiation from the ^1D state up to altitudes of ~ 250 km. Also, laboratory studies[14] of afterglow red line intensities suggest fast quenching of ^1D oxygen by O_2 molecules ($\beta > 10^{-11}$ cm^3/s). As we shall see, while quenching reactions may play an important role in determining the intensity of the radiation emitted, they do not affect the shape of the spectral line.

If fast excited atoms are produced by an electron-ion or atom-atom recombination reaction, one may still find an emitted line shape characteristic of the ambient gas temperature if ordinary recoil collisions with ambient atoms and molecules slow the fast excited atoms before they radiate. Since momentum transfer collision cross sections of $\sim 10^{-15}$ cm^2 are to be expected, at E-layer altitudes even the shorter-lived ^1S atoms would be "thermalized" by collisions before radiation could occur. In the case of the ^1D atoms, ambient densities above ~ 300 km are sufficiently small ($< 10^9$ cm^{-3}) that radiation before slowing may occur at these altitudes.

Finally, excitation transfer according to reactionsof the form

$$O_f^*(^1D) + O_s(^3P) \rightarrow O_f(^3P) + O_s^*(^1D) \quad , \qquad (5)$$

where the subscripts f and s refer to fast and slow atoms, respectively, may lead to loss of excitation by the fast atoms before they can radiate. Cross-sections for such resonant processes may be very large, although in several laboratory recombination studies involving excited states of neon and argon, cross-sections of only $\sim 10^{-15}$ cm^2 have been inferred from the measurements[4, 5]. Only if the resonant excitation transfer cross-section is reasonably small will fast ^1D oxygen atoms - with their 110 sec. lifetime - radiate before losing their excitation to slow O atoms in the F-region.

III. Possible Spectral Line Shapes

A. Thermal Doppler Line

The simplest line shape occurs when the excited atoms move with a velocity distribution characteristic of the ambient neutral temperature at the instant they radiate. In this case a gaussian profile of the type illustrated by the solid curve in Fig. 1(a) is to be expected for the emission of the λ6300 line by ^1D atoms (here, at a temperature of 950°K). The emitted line shape is unaffected by the ^1D excited atoms undergoing momentum transfer, excitation transfer, or quenching collisions. Momentum transfer collisions only maintain the ^1D atoms at the ambient neutral temperature, excitation transfer leads to excitation of ^3P oxygen atoms having the same (ambient) temperature, while those ^1D atoms which are quenched do not radiate at all. The dashed curve indicates the predicted effect on the line shape of instrumental broadening for a finesse, N = 8.1 (see Sec. V).

B. Simple Dissociative Line Shape

In the cases of production of ^1D (or ^1S) atoms by dissociative recombination of O_2^+ ions and electrons and by dissociative photoexcitation of O_2 by UV photons, rather peculiar line shapes are to be expected. The simplest case to discuss involves dissociative recombination production of the excited atoms.

Let us assume that the O_2^+ ions have a kinetic temperature equal to the ambient neutral temperature. If the recombination process proceeds from a particular (say v = o) vibrational state of the ion and involves capture of slow electrons, then, for a given branch in reaction (1), all of the ^1D atoms acquire a single speed, v_d, proportional to $(E_d)^{1/2}$, as they are repelled from the center of mass. Since, relative to an observer, all directions of dissociation are equally probable, the dissociation velocity vectors lie on the surface of a sphere, and it is a simple problem in geometry

to show that in the observor's (z) direction there is a uniform probability of finding a component of velocity v_z from $- v_d$ to $+ v_d$. Thus one expects a similar flat topped emission line shape over the frequency interval $\nu_o(1 - v_d/c)$ to $\nu_o(1 + v_d/c)$. When the thermal motion of the O_2^+ ion (center of mass) is considered, the predicted dissociative recombination line profile is given by (4, 15)

$$I(\tilde{\nu}) = (a/4b)\left[\operatorname{erf}(a\tilde{\nu} + b) - \operatorname{erf}(a\tilde{\nu} - b) \right] , \qquad (6)$$

where $a = (Mc^2/kT)^{1/2}/\nu_o$ and $b = (E_d/kT)^{1/2}$; $\tilde{\nu}$ and $\tilde{\nu}_o$ are the frequencies (in wave numbers), the subscript o referring to the line center, and M is the mass of the O atom. The predicted line shape is illustrated in Fig. 1(b) for the case of $E_d' = 3.1$ eV [the middle branch of reaction (1)] and $T = 950°K$. The dashed line indicates the effect of instrumental broadening on the observed line shape. If the several branches of reaction (1) all have a significant probability of occurrence, the line shape emitted would be expected to be a composite, involving superposition of the several widths corresponding to the different values of E_d.

The case of dissociative photoexcitation leads to a smearing of the simple profile described above, inasmuch as the Franck-Condon overlap region between the O_2 ground state and the repulsive branches of the excited O_2 molecule curves leads to absorption of photons of various energies and therefore to a continuum of E_d values over a certain energy range. However, since there may still be some minimum value of E_d imparted to the atoms (depending on the details of the repulsive potential curve), the emitted line may retain some of the characteristic "flat-topped" shape.

If the excited states with which we are dealing had sufficiently short radiative lifetimes, the atoms would radiate while they retained their

speed and excitation and thus the line shapes would be expected to exhibit the dissociative "signature". However, only under the most favorable circumstances can we hope to meet the required conditions, inasmuch as momentum transfer and excitation transfer cross sections as small as 10^{-15} cm^2 still permit collisional slowing of and loss of excitation by fast ^1D atoms before radiation at altitudes below 300 km. In these circumstances, thermal doppler line shapes at the ambient temperature would be noted, in spite of the fact that the atoms had been dissociatively produced.

The effect of a single momentum transfer collision on an idealized dissociative recombination line profile has been calculated[4] and is shown in Fig. 1(c). Evidently if the dissociatively produced excited atoms undergo a few momentum transfer collisions before radiation, the wings of the line appear more or less gaussian, while the line center retains a more flat-topped character.

C. Effects of Gross Motions of the Ionosphere

If the atmosphere containing the excited atoms exhibits some gross motion with respect to a fixed observor, e.g. as a result of the presence of winds, then the emitted lines will exhibit a frequency shift proportional to the component of wind velocity in the observor's direction. However, the Fabry-Perot interferometer used to determine the spectral line shapes does not readily permit precise absolute frequency determinations, and so such small shifts might go unnoticed. On the other hand, if the wind velocity components change markedly in passing through the emitting region, as a result of shear or velocity gradients, a slightly non-gaussion line, in some cases skew in shape about the line center, may be observed. This point is discussed further in analyzing the measurements (see Sec. V).

IV. Experimental Apparatus

The shapes of the λ6300 and λ5577 spectral lines are determined by means of a pressure-scanning Fabry-Perot interferometer[6, 7] employing photomultiplier detection and operating in either an output current or pulse counting mode. A simplified diagram of the apparatus is shown in Fig. 2. The large aperture (7.5 cm D) Fabry-Perot plates are mounted in an Invar frame, separated by a three-point Invar spacer (typically 7 mm in length). The plates are flat to λ/30 of Na D radiation and are coated with multilayer dielectric reflecting films giving reflectivities, R = 86%, 83%, and 81% at λ6300, λ5577, and λ5460 (calibrating Hg green line), respectively. The plates are enclosed in a pressure-tight, thermally insulated housing to permit variation of the index of refraction between the plates by controlled introduction of argon gas from a high pressure tank via an adjustable precision needle valve. The interference fringes are imaged by an aspherically corrected achromat (focal length = 49.0 cm) output lens onto a plate containing an aperture (0.229 cm D.) which is adjusted to coincide with the center of the fringes and thus pass a portion of the central spot to the detecting photomultiplier (E.M.I. type 9558 A). Thus, the photomultiplier output is proportional to the intensity of radiation having a wavelength given by the condition for constructive interference at the center of the pattern,

$$\lambda_{center} = 2\mu t/n \quad , \tag{7}$$

where λ_{center} is the wavelength measured in vacuum, μ is the index of refraction of the medium between the F-P plates, t is the plate spacing and n the interference order. Since the needle valve introduces gas from the high pressure tank to the housing at a constant rate, the wavelength (or frequency) of the radiation at the central spot changes linearly with time.

In order to reduce "noise", the photomultiplier is cooled to temperatures between 0°C and -80°C by means of dry ice inside an insulating housing. A further reduction in dark current pulses is obtained by use of a magnetic diverging lens[16] which reduces the effective photocathode surface from its diameter of 5 cm to ~ 4 mm by allowing multiplication down the tube only of those photoelectrons released from a small central spot on the photocathode. In this manner dark currents of $\sim 4 \times 10^{-13}$ amp. are obtained at the rated multiplier gain.

The desired oxygen line is separated from the rest of the airglow radiation by means of a 9Å half-width interference filter mounted ahead of the pressure housing. The entrance plate glass window to the housing is mounted at an angle so that a few percent of the radiation transmitted by the filter is reflected into a monitor photomultiplier. The portion of the sky observed by the instrument is controlled by a mirror, movable in azimuth and angle of elevation, mounted on top of the observatory. Calibration of the Fabry-Perot instrument's overall finesse is obtained by introducing radiation from an r-f excited isotopic mercury source so that it uniformly illuminates the full aperture of the instrument.

The apparatus is operated in two modes, as illustrated in Fig. 3. In the output current mode, the needle valve in Fig. 2 is adjusted so that argon gas is introduced into the Fabry-Perot housing at a rate which causes a line profile to be traced every ~ 10 min. (Each time the index of refraction increases sufficiently, the interference order increases by 1 and the line pattern repeats.) The output current is fed to an RC integrating network adjusted to reduce noise fluctuations without seriously distorting the line profile tracing. The output of the integrator is fed to a Keithley Type 600A electrometer whose output drives the y-axis of a chart recorder. (A second channel in this recorder is driven by the monitor photomultiplier

output.) The x-axis of the chart is driven by a synchronous motor so that the chart record is effectively a linear presentation of I vs λ or $\tilde{\nu}$.

Improved signal averaging, without distortion of the line shape, has been obtained by operating in a pulse counting mode and adjusting the needle valve to tune the interferometer through one interference order in $\sim$1 min. A cyclical pressure scan is introduced by use of a 1 r.p.m. synchronous motor (s.m.) which opens a fast pressure release valve once a minute. The pulses from the photomultiplier are fed through a preamplifier to the amplifier and discriminator section of a TMC Model 102 Multichannel Analyzer, which is set to advance channels at the rate of 1 per sec, starting at the instant the fast release valve closes (tripping a micro-switch) and stopping when the valve opens 57 sec later. In this manner the spectral line is scanned once a minute and as many scans as desired can be accumulated in the memory of the multichannel analyzer. Readout of the stored data is made in analogue form on a strip chart recorder and in digital form on a printer.

In order to evaluate the performance of the Fabry-Perot etalon and to analyze the experimentally observed line profiles, computations have been made[17] of the expected line contours taking into account the figuring of the plates (assuming spherical departure from flatness), the reflection coefficient of the dielectric films, and the finite aperture in the image plane. For our apparatus observing the isotopic Hg λ5460 line, an overall finesse, N (equal to the free spectral range divided by the width at half intensity), of 9.06 is predicted, in agreement with the measured value, under optimum adjustment, of 9.0 obtained during 1966 observations. The apparatus was dissassembled for modification during January-April 1967, and since that time the best instrumental finesse achieved has been 8.1. The predicted instrumental line shapes for both the finesse 9.0 and 8.1

agree quite well with the measured shapes using the isotopic Hg calibrating source.

V. Results and Discussion

Studies of the nightglow line shapes have been carried out at the University of Pittsburgh's Airglow Observatory atop Laurel Ridge (elevation 2700 ft., 79° 10' W. Long., 40° 10' N. Lat.) approximately 50 miles southeast of Pittsburgh, Pennsylvania. The results of the observations to date reveal the following:

(a) In no case is any evidence found for a dissociative line shape in λ6300.

(b) Most of the λ6300 line profiles have thermal doppler shapes, from which we have obtained the temperature of the $O(^1D)$ atoms as a function of time after sunset.

(c) There is the possibility, in one set of observations, that wind shear effects have been detected, in that slight frequency shifts and asymmetrical line shapes have been noted.

(d) Green line (λ5577) temperatures are rather poorly determined with the present, moderate finesse apparatus.

We shall now discuss these various observations in detail.

An example of the observed λ6300 line profile on a "hot" night is shown in Fig. 4. In most of these observations the line of sight of the instrument has been in the sunset direction, W to NW, and at an elevation angle between 25° and 30°. It will be seen that the data fall quite well on the predicted profile for a doppler line at a temperature T = 1580°K convoluted with the instrumental function for the measured finesse, $N_{Hg} = 8.1$. The I-shaped symbols indicate the statistical fluctuations, $\pm\sqrt{c}$, where c is the number of counts in a given channel, which are to be

expected in the data. In view of the uncertainties in the data, the derived temperature in this case is probably accurate to better than ± 100°K.

Some examples of the variation of $O(^1D)$ atom temperature with time, deduced from the λ6300 line widths, are shown in Figs. 5-8. It is assumed that the bulk of the nightglow λ6300 radiation emanates from heights $\gtrsim$ 200 km[1] and so provides a direct determination of the ambient neutral temperature above the thermopause. The maximum uncertainty in the temperatures deduced from the line widths is estimated to be $\sim(\pm$ 150)°K, the minimum $\sim(\pm$ 50)°K. In all cases the data shown indicate either an essentially constant or a slowly falling ($\sim$50°K/hr) temperature until late in the night ($\sim$03:00). The lines in the figures are the predictions of the analysis of Jacchia[18], who established a correlation between solar decimeter flux and geomagnetic activity and the exospheric temperature deduced from satellite drag. These "theoretical" lines represent the temperature predicted using only the decimeter flux ($F_{10.7}$) in Jacchia's analysis. The additional temperature rise due to geomagnetic activity[18] (K_p indices) is found to be small ($\lesssim$ 50°K) for those nights for which the indices are currently available and therefore has been omitted from the curves.

It will be seen that on June 1 and August 29/30, 1967 the Jacchia model predicts the observed temperatures quite well, and in addition predicts the observed trend to higher temperatures between May 18 and June 1, 1967. However, a rather stronger decrease in exospheric temperature was noted between June 5-6 and June 27 ($\sim$400°K) than is predicted from Jacchia's model (< 100°K).

In the fall of 1966 the exospheric temperatures were found to be lower ($\lesssim$ 900°K) than in the spring and summer of 1967, in accordance with the predictions of the model. Further, the model predicted substantially the same temperature for Oct. 20 and Nov. 15/16, in agreement with the

observations, although the model temperature was ~150°K higher than the observed. However, the predicted temperature for Oct. 12 was within 20°K of the values for Oct. 20 and Nov. 15/16, while the measurements indicated that it was substantially (~300°K) lower. Thus, on occasion, we observe F layer temperatures which differ substantially from the predicted exospheric temperatures derived from solar activity.

The predicted diurnal variation of exospheric temperature was confirmed, within experimental error, by our observations of Aug. 29/30, 1967, the data indicating a gradual temperature fall to late night, followed by a slow rise toward morning (see Fig. 8). The only serious anomaly in these data occurred at 00:54, when a higher temperature was deduced from a rather poorer line shape (note the error bar). We mention this anomaly because there has been a preliminary report of a similar sudden, late night temperature increase deduced from radar measurements of Thomson scattering(19).

Finally, a rather interesting set of λ6300 line profiles, which were obtained on Nov. 13, 1966, is shown in Fig. 9. The first profile, obtained by accumulating seven one minute scans centered at 17:33 local solar time, shows the sloping background of the darkening sky, but the line is otherwise symmetrical. This is confirmed by the 13 scans centered at 17:50, which yield a symmetrical line on a uniform "dark sky" background. Both profiles have the same center frequency (at the equivalent channel number 37 1/2 of the multichannel memory). The next three profiles exhibit both a center frequency shift and a slight asymmetry in shape. The first, obtained with 6 scans centered at 18:18, has an anomalously high counting rate, ~220 counts/s, at peak intensity compared to ~70 counts/s at 17:50 and 40 counts/s at 18:34. However, even if we ignore this profile, those obtained at 18:34 (7 scans) and at 18:58 (23 scans) exhibit slight center frequency shifts and asymmetries, while yielding more normal photon counting rates. (The dashed lines indicate

the folded, symmetrical continuation of the left hand sides of the curves.) The center frequency shift requires a velocity toward the observor (i.e. to the east) of $\sim$400 m/s, while the asymmetry requires that a substantial wind shear or velocity gradient occur through the emitting F-layer, so that a part of the emitting region exhibits no pronounced motion with respect to the observor. There are some indications that F layer wind velocities of this magnitude are possible[20]. On one occasion (March 5, 1960) Blamont and Baquette[20] observed a sharply increasing wind velocity with increasing altitude, a value $\sim$200 m/s being recorded at the highest altitude for which measurements were obtained (170 km). In addition, a strong velocity gradient, $\sim$4 m/s per km, was noted between 130 and 170 km.

At the present time, our observations of green line (λ5577) profiles are not sufficiently accurate to yield reliable temperature determinations, owing to insufficient instrumental finesse (N$\sim$8-9). The results of analysis of the few observations which yielded good line profiles are summarized in Table I. There was noticeable auroral activity visible in the northern sky on the night of Nov. 15, 1966, which faded as the night progressed. Thus, the observation of temperatures of 480 and 370°K when looking into the active zone and of 200°K when looking at the ordinary nightglow are consistent with other determinations of the nightglow[21] and auroral[22] green line temperatures.

VI. Conclusions

Up to the present we have been unable to detect evidence for the dissociative production of $O(^1D)$ atoms in the measured λ6300 line profiles. (In all cases, the line shapes are consistent with a thermal doppler shape or exhibit a skewness which may arise from wind effects.) This is not to be taken as evidence against such a dissociative origin, since collisional slowing of and excitation transfer by the dissociatively produced atoms are

Table I Green line (λ5577) temperatures on Nov. 15/16, 1966

(observations at 30° elevation angle)

local solar time	observing direction	Temperature (°K)
19:45	W	200 ± 40
20:00	W	200 ± 40
20:15	N	480 ± 50
02:30	N	370 ± 50

expected to lead to profiles which are nearly gaussian, except under unusually favorable conditions.

We are currently fabricating a larger (10 cm aperture) Fabry-Perot etalon designed to provide greatly improved overall finesse ($N \geq 25$) in order to examine in more detail the structures of the λ6300 and λ5577 line profiles. In this way we hope to be able to detect smaller remnants of the dissociative "signature" in the presence of a large thermal doppler core. In addition, more precise center frequency determinations will permit us to establish whether or not gross motions due to wind are occurring in the emitting layers of the upper atmosphere.

The improved instrument should also reduce our errors in the exospheric temperature measurements and so permit more meaningful determinations of temperature variation during the night. At the present time it appears that the empirical models[18, 23, 24] of the exospheric temperature (based on analysis of satellite drag data in terms of atmospheric heating due to solar activity) do not fully explain the F layer temperatures deduced from the λ6300 line width determinations, both in the present work, and in that of Jarrett and Hoey[8].

In order to provide simultaneous F-layer temperature determinations by more than one method, coordinated measurements of λ6300 line widths and radar Thomson scattering[25] are planned. In this way it will be possible to compare the directly determined excited atom temperatures with the ambient temperatures inferred from the F-layer electron and ion temperature determinations of the radar backscatter method[25].

The authors are greatly indebted to Mr. R. Hake, who carried out the computer line profile analyses and assisted with data taking. They also wish to thank their colleagues, especially T. M. Donahue, for valuable discussions of such subjects as ionospheric excitation processes and exospheric temperature models.

References

1. J. W. Chamberlain, Physics of the Aurora and Airglow, (Academic Press, New York and London, 1961).
2. F. E. Roach, "The Nightglow", in Adv. in Electronics and Electron Physics, Vol. 18, L. Marton, Ed. (Academic Press, New York and London, 1963).
3. W. H. Kasner and M. A. Biondi, Bull. Am. Phys. Soc. 12, 218 (1967).
4. T. R. Connor and M. A. Biondi, Phys. Rev. 140, A778 (1965).
5. L. Frommhold and M. A. Biondi, Bull. Am. Phys. Soc. 11, 493 (1966).
6. P. Jacquinot and C. Dufour, J. Rech. 6, 91 (1948).
7. M. A. Biondi, Rev. Sci. Inst. 27, 36 (1956).
8. A. H. Jarrett and M. J. Hoey, J. Atmos. Terrest. Phys. 28, 175 (1966).
9. A. Dalgarno and J. C. G. Walker, J. Atmos. Sci. 21, 463 (1964).
10. J. C. G. Walker, J. Atmos. Sci. 19, 1 (1965).
11. D. M. Hunten, Space Science Rev. 6, 493 (1967).
12. K. D. Cole, Ann. Geophys. 21, 156 (1965).
13. D. R. Snelling and E. J. Bair, J. Chem. Phys. 47, 228 (1967).
14. E. C. Zipf, Bull. Am. Phys. Soc. 12, 225 (1967)
15. W. A. Rogers and M. A. Biondi, Phys. Rev. 134, A1215 (1964).
16. L. Frommhold and W. A. Feibelman, J. Sci. Instrum. 44, 182 (1967).
17. R. Hake, private communication. This computer calculation is evidently similar to that of K. Krebs and A. Sauer, Ann. Phys. 13, 359 (1953).
18. L. G. Jacchia, Ann. d. Geophys. 22, 75 (1966).
19. P. Waldteufel, private communication.
20. J. E. Blamont and J. M. Baguette, Ann. Geophys. 17, 319 (1961).
21. D. M. Hunten, Ann. Geophys. 17, 249 (1961).
22. E. B. Armstrong, J.A.T.P. 13, 205 (1959).
23. L. G. Jacchia and J. Slowey, J. Geophys. Res. 72, 1423 (1967).

24. I. Harris and W. Priester, J. Geophys. Res. 67, 4585 (1962).

25. J. S. Nisbet, "Neutral Atmospheric Temperatures from Incoherent Scatter Observations", Pennsylvania State Univ. Ionospheric Research Report No. 290, Feb. 16, 1967, unpublished.

Figure Captions

Fig. 1 Solid curves: Predicted λ6300 line shapes showing doppler effects due to thermal motion and dissociative recombination. Dashed curves: Predicted effect on the line shape of instrumental broadening at a finesse $N_{Hg} = 8.1$ (see text for details).

Fig. 2 Simplified diagram of pressure scanned Fabry-Perot interferometer.

Fig. 3 Simplified block diagram of the overall apparatus used to obtain spectral line shapes.

Fig. 4 Observed λ6300 line profile on June 5, 1967 compared to predicted shape for an excited atom-temperature of the 1580°K and an instrumental finesse $N_{Hg} = 8.1$. The I-shaped symbols indicate the expected statistical fluctuations in the data.

Fig. 5 F-layer temperature vs local solar time inferred from λ6300 line widths on Oct. 12 and 20 and Nov. 15/16, 1966. The solid line represents the predicted temperatures on those dates using the model of Jacchia.

Fig. 6 F-layer temperature vs local solar time on May 18 and June 1, 1967. The error bars shown for the two points indicate the magnitude of the uncertainty in the data for these two nights. The solid lines represent the predictions of Jacchia's model.

Fig. 7 F-layer temperature vs local solar time on June 5, 6, and 27, 1967. The error bars shown apply to most of the data points. The solid lines represent the predictions of Jacchia's model.

Fig. 8 Observed F-layer temperature vs local solar time on Aug. 29/30, 1967 compared with the predictions of Jacchia's model. The open circle labelled Z was taken pointing at the zenith. The estimated temperature errors for the data points are $\sim \pm$ 50°K, with the exception

of the three points with the error bars, which were somewhat less certain.

Fig. 9 λ6300 line shapes observed on November 13, 1966, indicating possible F-layer wind effects. The numbers inside circles indicate the number of scans of the spectral line accumulated in the multi-channel analyzer's memory.

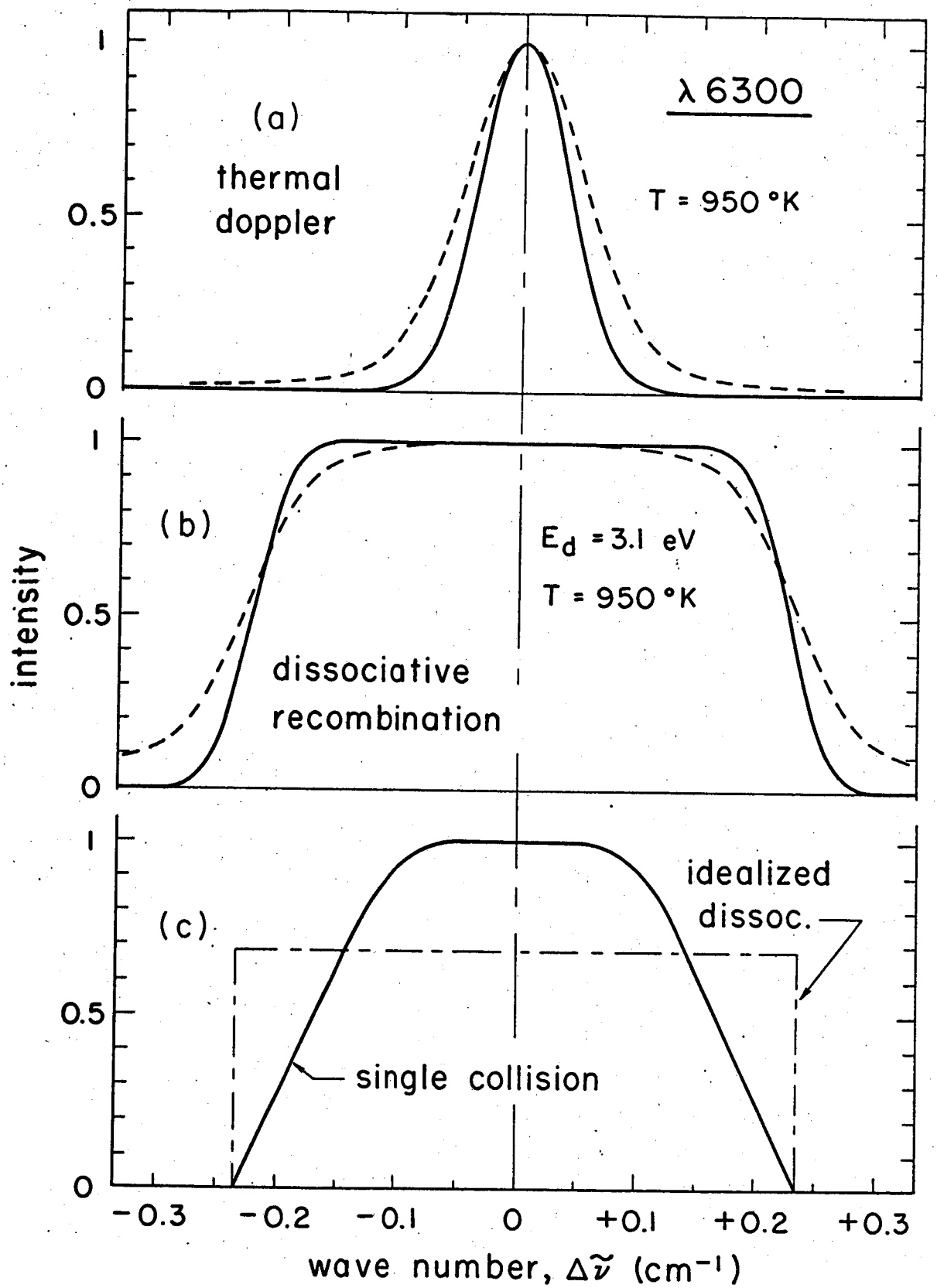
(a)
thermal
doppler
λ 6300
T = 950 °K
(b)
E_d = 3.1 eV
T = 950 °K
dissociative
recombination
(c)
idealized
dissoc.
single collision
intensity
1
0.5
0
−0.3
−0.2
−0.1
0
+0.1
+0.2
+0.3
wave number, $\Delta\tilde{\nu}$ (cm^{-1})

Figure 1

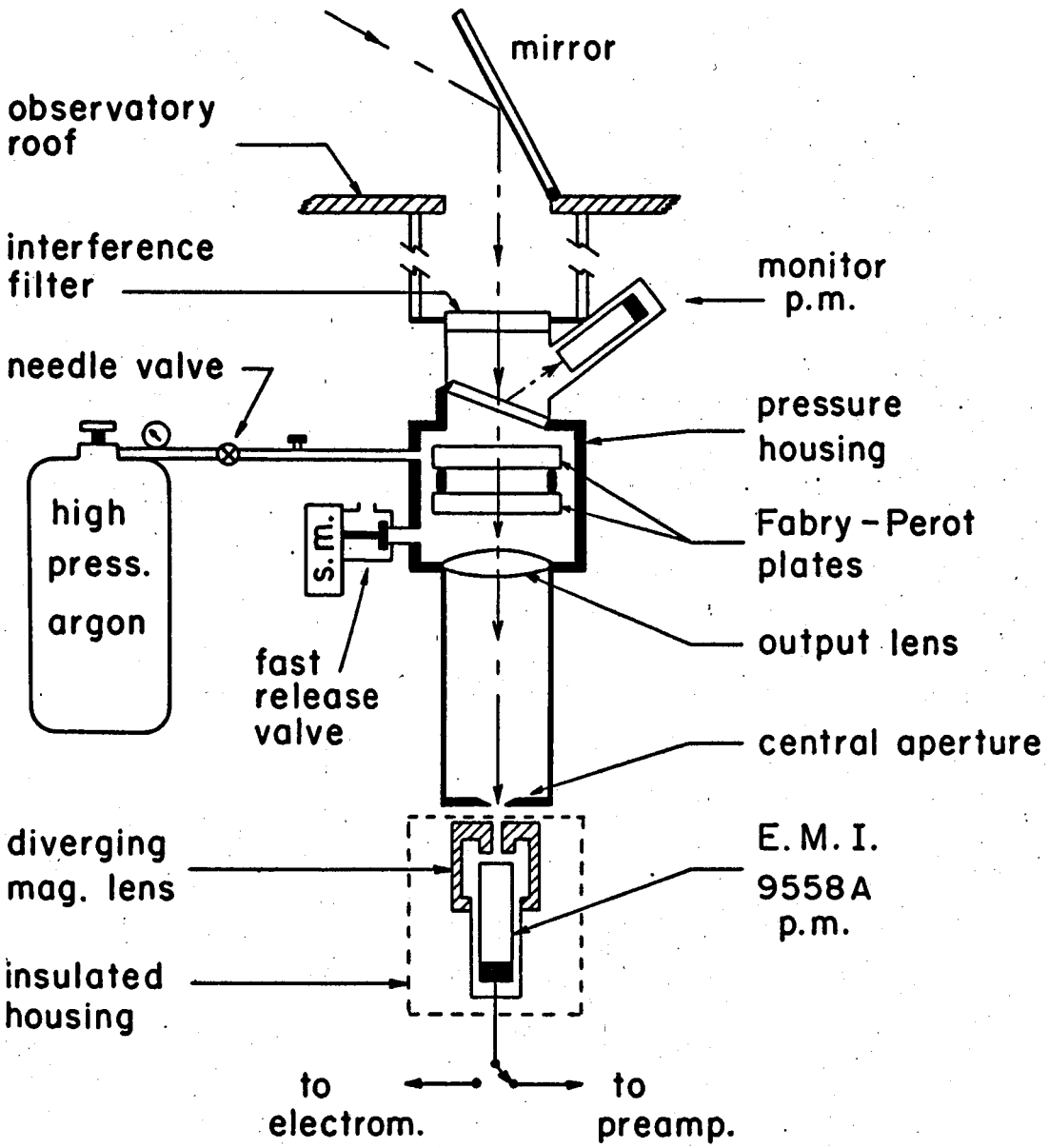
mirror
observatory roof
interference filter
monitor p.m.
needle valve
pressure housing
high press. argon
S.M.
Fabry-Perot plates
output lens
fast release valve
central aperture
diverging mag. lens
E.M.I. 9558A p.m.
insulated housing
to electrom.
to preamp.

Figure 2

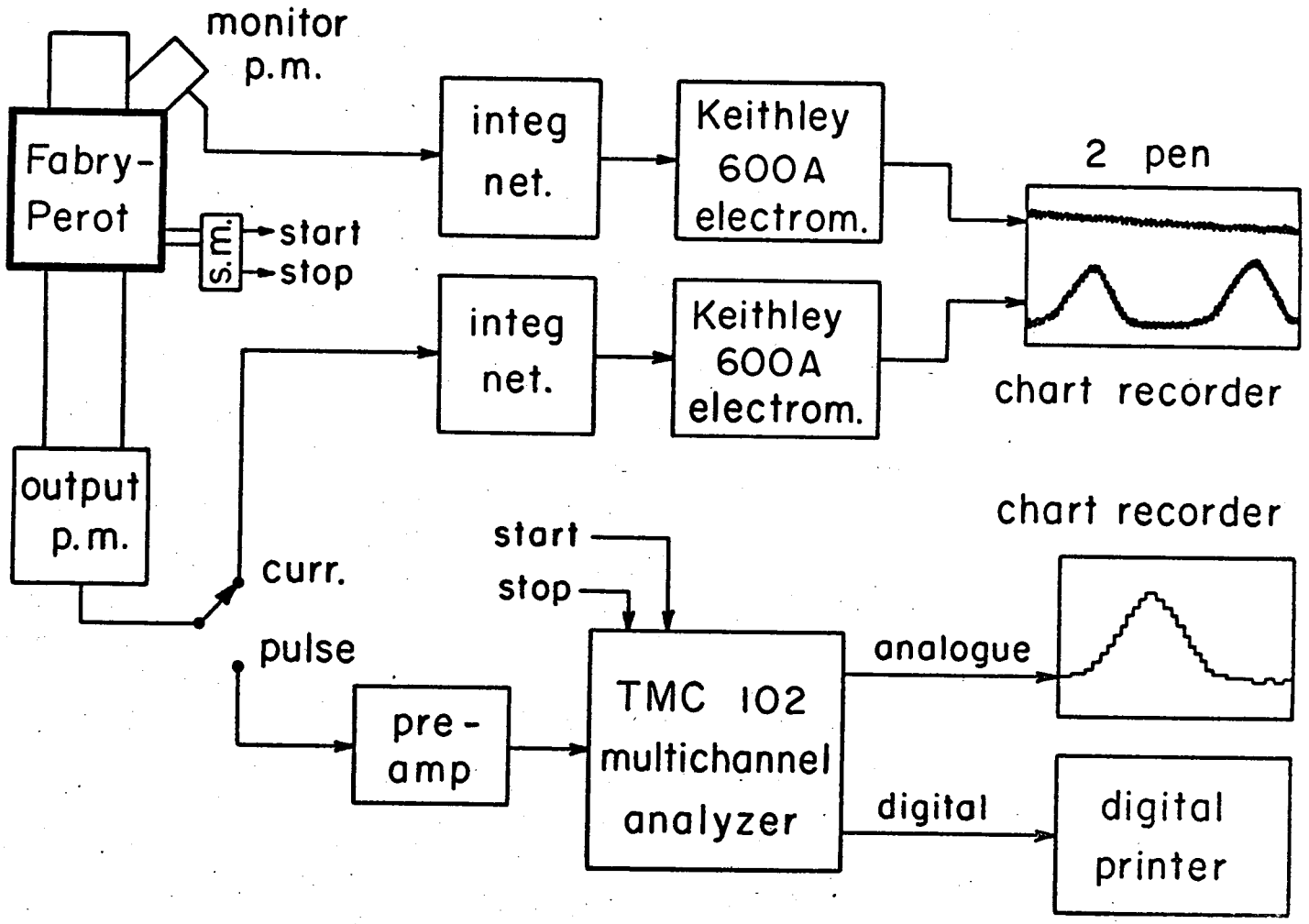
monitor
p.m.
Fabry-
Perot
s.m.
start
stop
integ
net.
Keithley
600A
electrom.
2 pen
integ
net.
Keithley
600A
electrom.
chart recorder
output
p.m.
curr.
pulse
start
stop
chart recorder
pre-
amp
TMC 102
multichannel
analyzer
analogue
digital
digital
printer

Figure 3

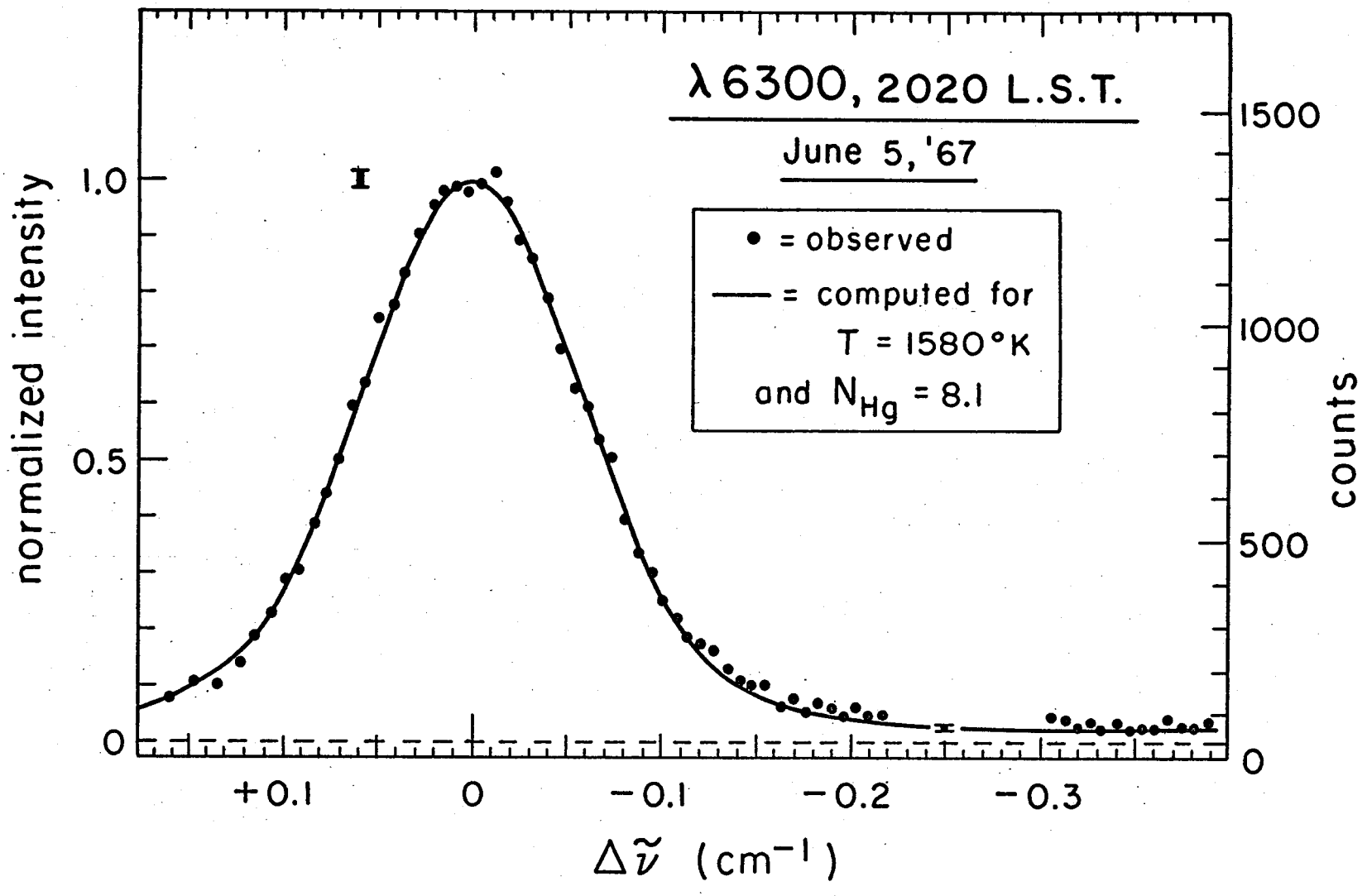
λ6300, 2020 L.S.T.
June 5, '67
• = observed
—— = computed for
T = 1580°K
and N_{Hg} = 8.1
normalized intensity
1.0
0.5
0
counts
1500
1000
500
0
+0.1
0
−0.1
−0.2
−0.3
$\Delta\tilde{\nu}$ (cm^{-1})

Figure 4

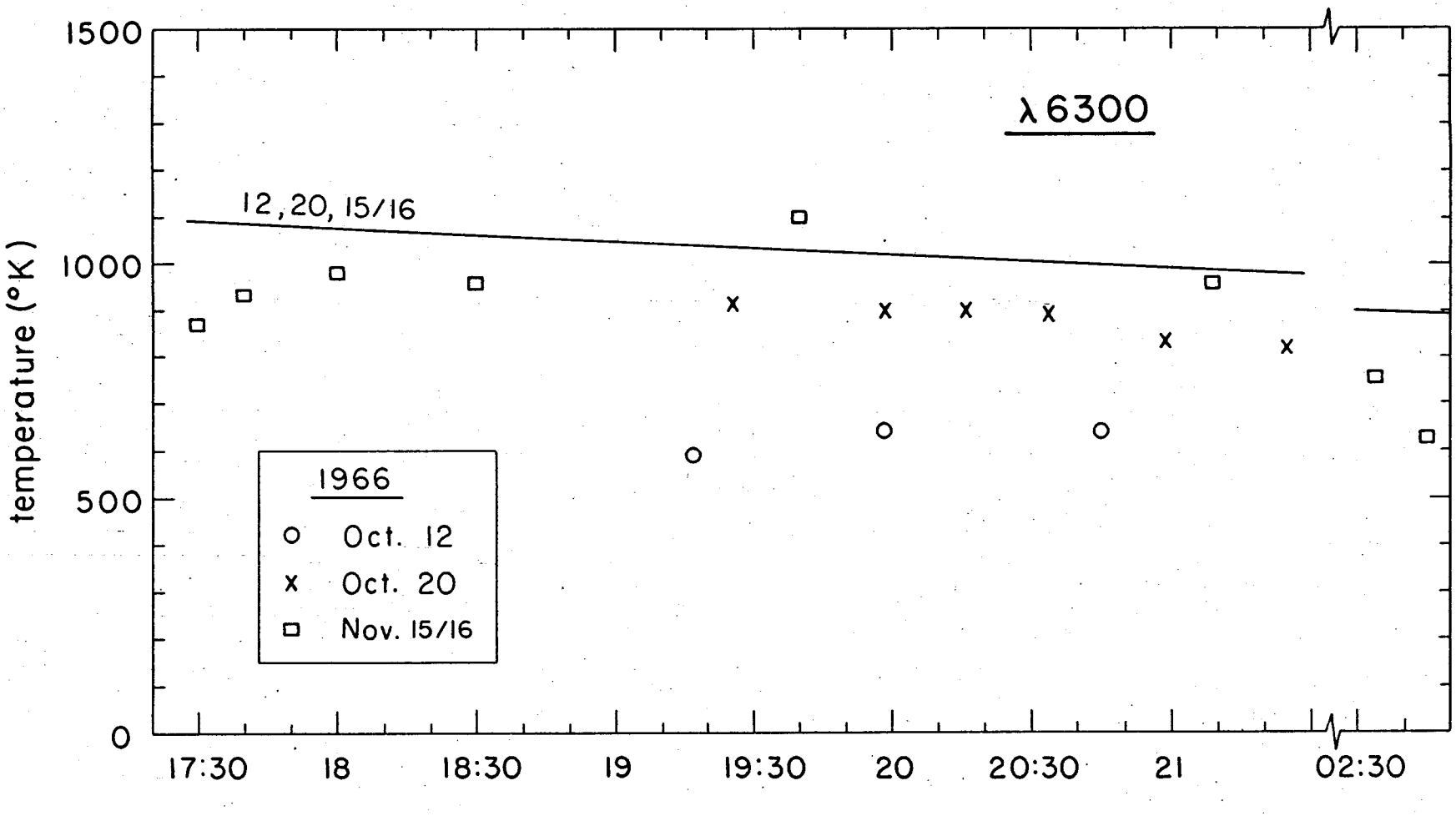
λ6300
12, 20, 15/16
1966
Oct. 12
Oct. 20
Nov. 15/16
temperature (°K)
1500
1000
500
0
17:30
18
18:30
19
19:30
20
20:30
21
02:30
local solar time

Figure 5

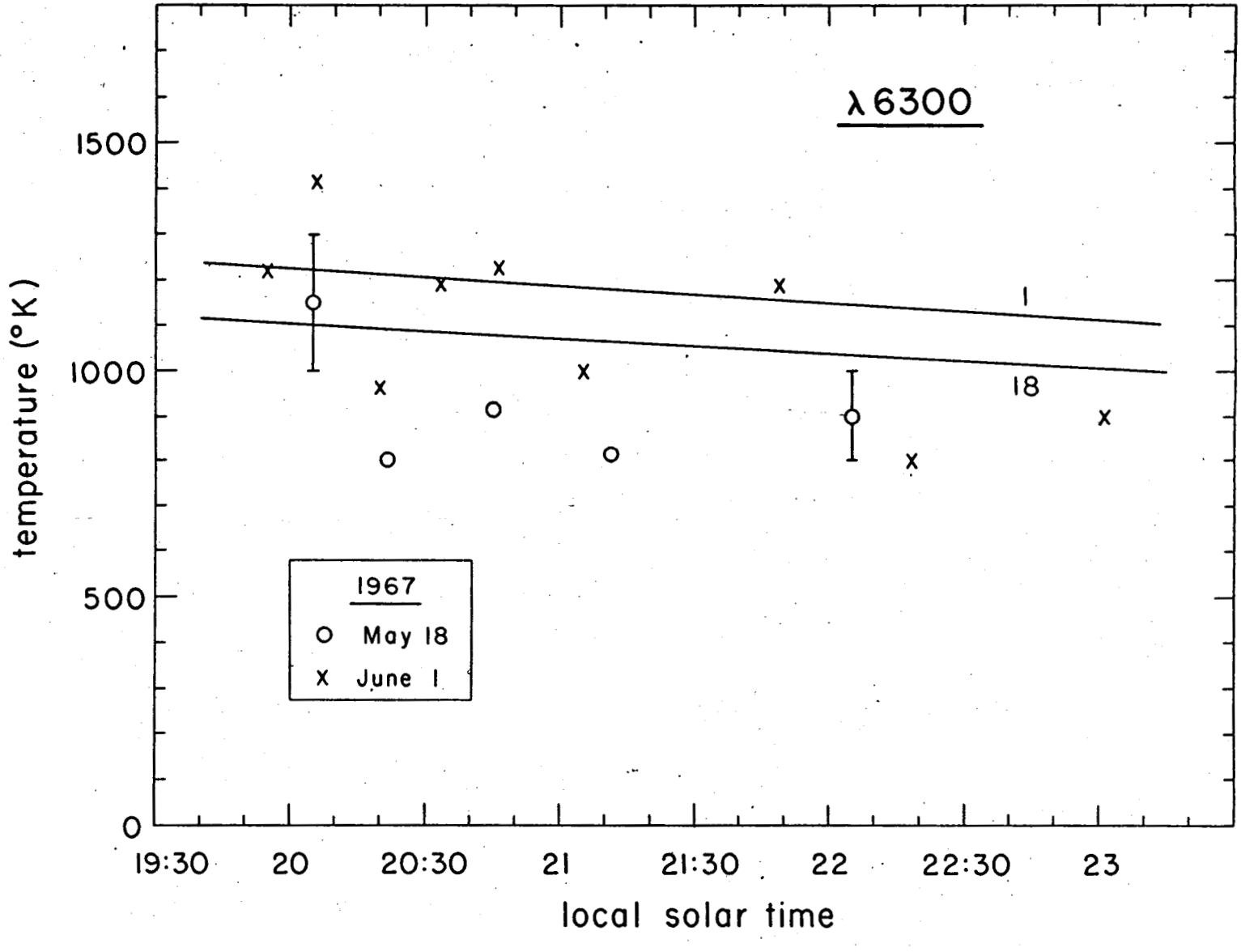
λ6300
1500
1000
500
0
temperature (°K)
19:30
20
20:30
21
21:30
22
22:30
23
local solar time
1967
May 18
June 1
18
1

Figure 6

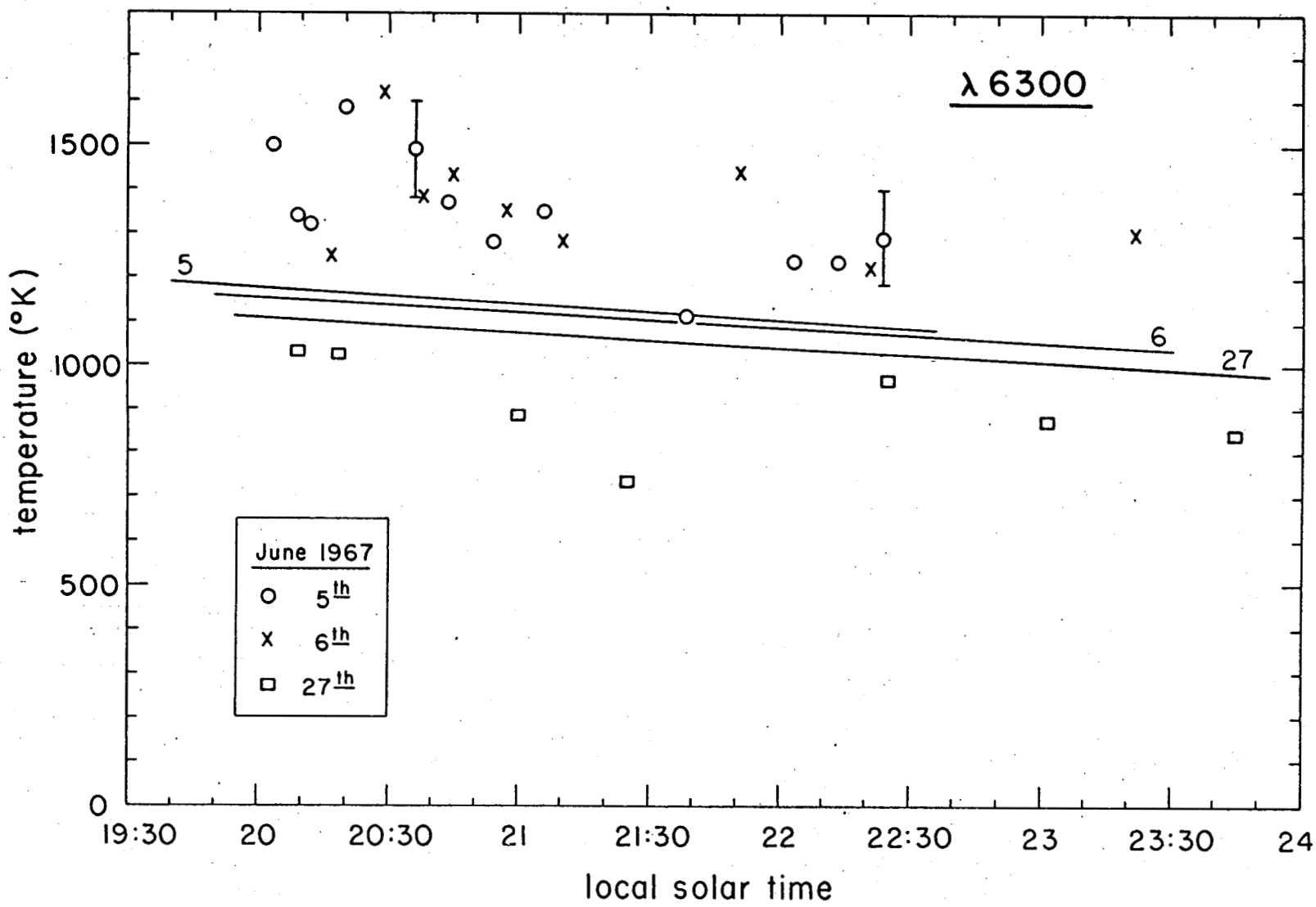
λ 6300
1500
1000
500
0
temperature (°K)
5
6
27
June 1967
5th
6th
27th
19:30
20
20:30
21
21:30
22
22:30
23
23:30
24
local solar time

Figure 7

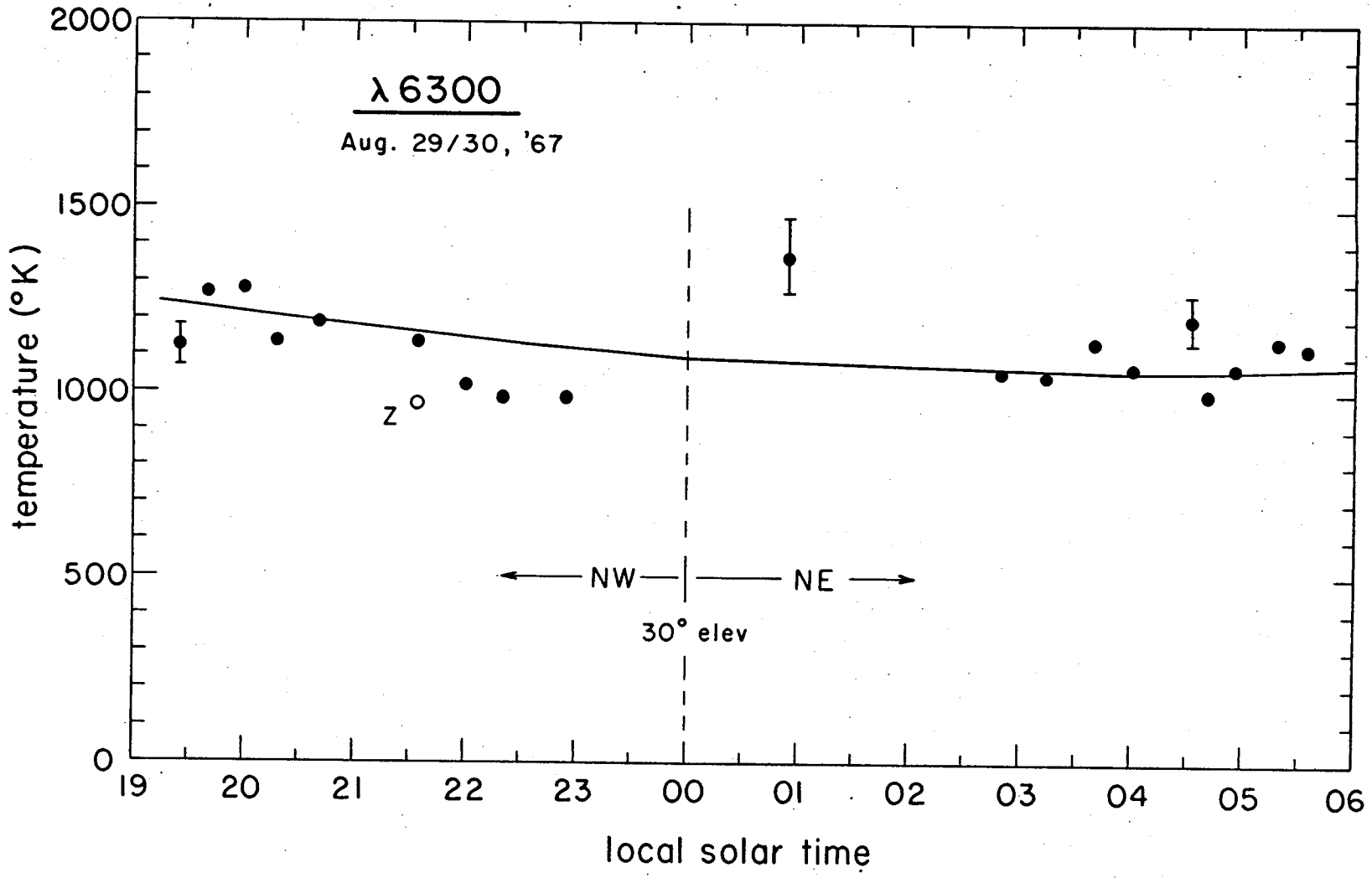
λ6300
Aug. 29/30, '67
2000
1500
1000
500
0
temperature (°K)
Z °
NW
NE
30° elev
19
20
21
22
23
00
01
02
03
04
05
06
local solar time

Figure 8

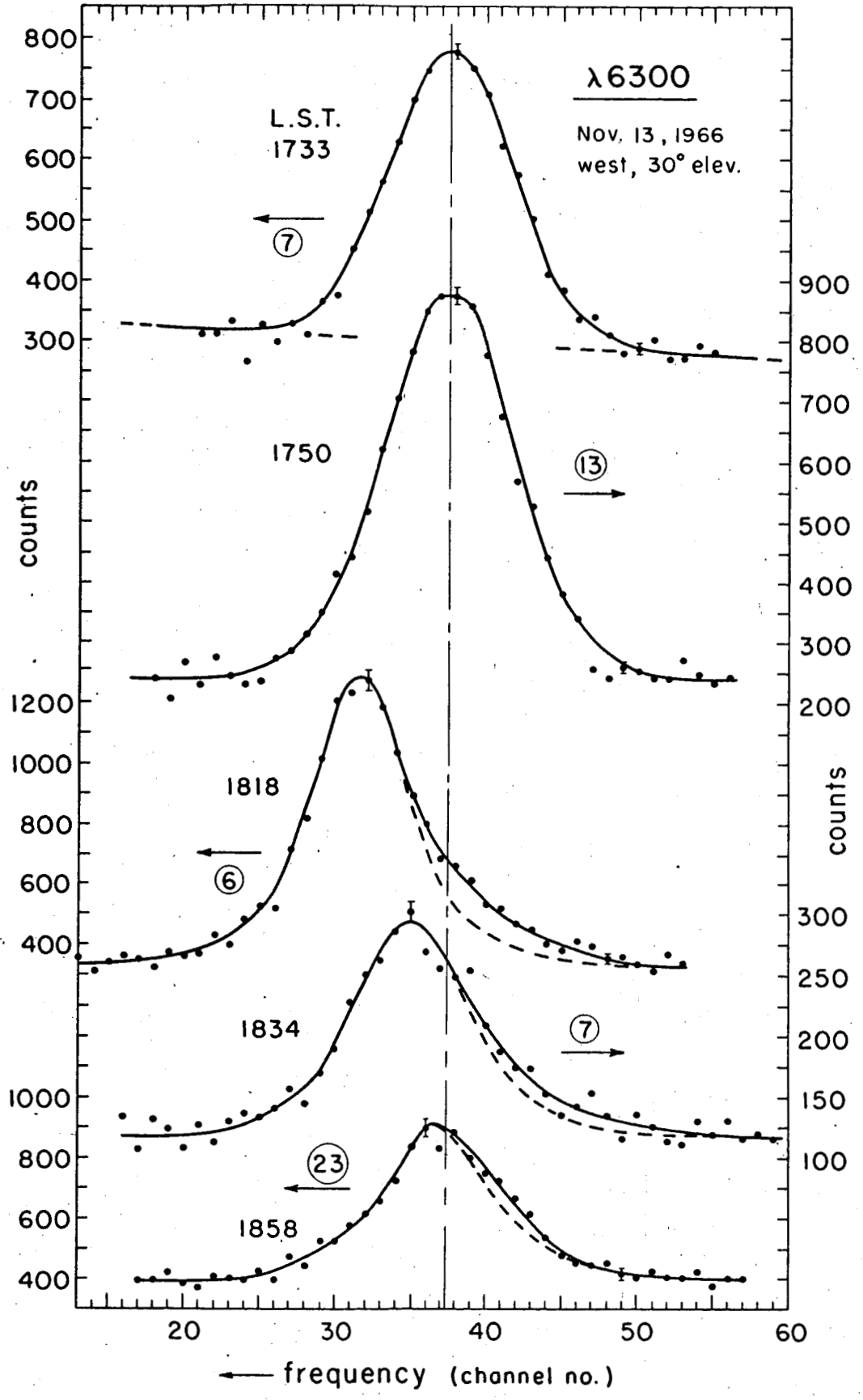
λ6300
Nov. 13, 1966
west, 30° elev.
L.S.T.
1733
⑦
1750
⑬
1818
⑥
1834
⑦
1858
㉓
counts
counts
frequency (channel no.)
20
30
40
50
60

Figure 9